Hybrid planar free-electron maser in the magnetoresonance regime

Vitaliy A. Goryashko and Kostyantyn Ilyenko*
Institute for Radiophysics and Electronics of NAS of Ukraine, 12 Acad. Proskura Street, Kharkiv, 61085, Ukraine

Anatoliy Opanasenko
National Science Center "Kharkiv Institute of Physics and Technology" of NAS of Ukraine, 1 Akademichna Street, Kharkiv, 61108, Ukraine

(Received 7 July 2008; published 7 October 2009)

We study the operation regime of a hybrid planar free-electron maser (FEM) amplifier near the magnetoresonant value of the uniform longitudinal (guide) magnetic field. Using analytical expressions for individual test electron trajectories and normal frequencies of their three-dimensional oscillations in the magnetostatic field of the hybrid planar FEM, an analytical condition of chaotization of motion is established and shown to be given by the Chirikov resonance-overlap criterion applied to the normal undulator and cyclotron frequencies with respect to the coupling induced by the undulator magnetic field. It is also shown analytically that, in spite of the well-known drop for the exact magnetoresonance, the gain attains its maximal value in the zone of regular dynamics slightly above the magnetoresonant value of the guide magnetic field. Under the condition of undulator resonance, it is practically independent of the amplitude of the undulator magnetic field and the wavelength of amplified signal. To account for space-charge effects, we propose a theoretical model of a weakly relativistic FEM, which accommodates not only potential but also rotational parts of the nonradiated electromagnetic field of a moving charged particle. It turns out that the rotational part of nonradiated field diminishes the defocusing influence of the potential part on the beam bunching. Numeric simulation of the nonlinear stage of amplification is fulfilled, taking into consideration adiabatic entrance of the electron beam to the interaction region and initial electron velocity spread. We find that nonradiated field and initial electron velocity spread do not influence essentially the efficiency of hybrid planar FEM amplification if parameters of the beam-microwave interaction correspond to the operational regime in the zone of regular dynamics near the magnetoresonance.

DOI: 10.1103/PhysRevSTAB.12.100701 PACS numbers: 84.40.Ik, 34.80.Qb, 05.45.−a, 41.60.Cr

I. INTRODUCTION

Starting with the successful experiment [1,2], the previous three decades have witnessed a spectacular development of theory and experiment of a free-electron maser with a guide (uniform longitudinal) magnetic field [hybrid free-electron maser (FEM)]. Utilizing the Doppler frequency upshift, free-electron masers and lasers possess a unique property to amplify and generate coherent electromagnetic radiation across the nearly complete electromagnetic spectrum: from radio waves to vacuum ultraviolet [3]. An interest in the hybrid FEM is reinforced by a promise to attain a substantial microwave power level (up to a few gigawatts) in their planar configuration because of the use of superwide sheet electron beams (e.g., in [4] emission and transport of a 140 cm-wide, 20 kA and 2 MeV sheet electron beam for purported FEM applications was reported). Sheet electron beams allow one to weaken restrictions on the maximal aggregate beam current posed by space-charge effects while reaching the current values of about $30 \div 50$ kA. This makes the hybrid planar FEM one of the most attractive sources of powerful electromagnetic radiation in the terahertz gap: the frequency range from 0.3 to 3 THz.

In pioneering works [5–9] analytical investigations of stationary regimes of microwave amplification and generation in a hybrid FEM were carried out; later these results were refined mainly through numerical simulations. Experimentalists [10–13] reported a considerable loss of electron beam current and microwave power for a hybrid FEM for a certain range of values of the guide magnetic field. A study of chaotic particle dynamics in free-electron lasers was undertaken in papers [14,15], where the authors investigated effects of the high-current (high-density) regime and the transverse spatial gradients in the applied wiggler magnetostatic field, and in Refs. [16,17], where the motion of an individual test electron in the (''ideal'') magnetostatic field of the hybrid planar FEM was found to be nonintegrable. Nevertheless, to the present day there still exist some fundamental questions, which either have no answers or only partial ones (cf. [18], pp. 430–439): under what conditions motion of an individual test electron

*kost@ire.kharkov.ua

becomes chaotic in the presence of the guide magnetic field; what does influence the width of dynamical chaos zone around the magnetoresonant value (the undulator frequency is approximately equal to the cyclotron frequency) of the guide magnetic field; what does define the maximal value of the gain under the conditions of the magnetoresonance; and, finally, how do beam initial parameters spread and space-charge effects impact microwave amplification?

We focus our attention on the operation of FEM around the magnetoresonant regime caused by the guide magnetic field usually used in FEM setups to enhance the efficiency of beam-microwave interaction and provide transverse confinement of the electron beam. The study is based upon analytical asymptotically exact expressions for electron trajectories developed recently [19] as well as on the use of numerical simulations. More specifically, in the adopted approach we highlight the fundamental role of the nonlinear dynamical system describing motion of electrons in the combined magnetostatic spatially periodic (undulator) and uniform guide magnetic field.

The next section contains a nonlinear self-consistent system of equations governing a hybrid planar FEM amplifier. In Sec. III, we find asymptotically exact solutions of equations of motion of an individual test electron in the magnetostatic field of a hybrid planar FEM and study their properties. Section IV contains the dispersion equation and calculation of magnetoresonant growth rate under the undulator resonance. In Sec. V, we accomplish numerical simulations of the self-consistent nonlinear system of governing equations and study the impact of beam initial velocity spread and space-charge effects. The article ends with the Sec. VI.

II. GOVERNING EQUATIONS

We regard that at the entrance of the interaction region (cross section $z = 0$) of a hybrid planar FEM, the electron beam is continuous and unmodulated. In the amplifier regime there is also a seed microwave signal. It can be shown that for a regular electrodynamics structure the microwave field and electron beam current density in the interaction region are periodic functions of time. Neglecting temporal harmonics generation of the microwave field, we consider the case such that there occurs resonant interaction only with one spatial harmonic of the microwave field. Under such assumptions we write the microwave and nonradiated (space-charge) field in an ideally conducting regular waveguide with the electron beam as follows:

$$\vec{E}(\vec{r},t) = \mathrm{Re}\{C(z)\vec{e}(\vec{r}_\perp)e^{-i(\omega t-k_z^0 z)}\} - \vec{\nabla}\varphi - \frac{1}{c}\frac{\partial \vec{A}^{qs}}{\partial t},$$
$$\vec{B}(\vec{r},t) = \mathrm{Re}\{C(z)\vec{b}(\vec{r}_\perp)e^{-i(\omega t-k_z^0 z)}\} + \vec{\nabla}\times\vec{A}^{qs}, \qquad (1)$$

$$\frac{dC}{dz} = -\frac{\omega}{4\pi P_0}\int_S\int_{-\pi/\omega}^{+\pi/\omega}[\vec{j}^r(\vec{r},t)\cdot\vec{e}(\vec{r}_\perp)^*] \times e^{i(\omega t-k_z^0 z)}dtdS;$$
$$\triangle\varphi(\vec{r},t) = -4\pi\varrho(\vec{r},t), \qquad (2)$$
$$\vec{j}^r = \vec{j} - \frac{1}{4\pi}\frac{\partial}{\partial t}\vec{\nabla}\varphi,$$
$$\triangle\vec{A}^{qs}(\vec{r},t) = -\frac{4\pi}{c}\vec{j}^r(\vec{r},t);$$

$C(z)$ is the (slowly varying) amplitude of the microwave; $\vec{e}(\vec{r}_\perp)$ and $\vec{b}(\vec{r}_\perp)$ are the membrane eigenfunctions of the coordinates $\vec{r}_\perp = (x, y)$ in the waveguide cross section S (microwaves and the electron beam propagate in the positive direction of the z axis, see Fig. 1); k_z^0 is the "cold" propagation constant of the eigenwave; the star $(*)$ denotes complex conjugation:

$$P_0 = \frac{c}{8\pi}\,\mathrm{Re}\int_S\{[\vec{e}(\vec{r}_\perp)\times\vec{b}^*(\vec{r}_\perp)]\cdot\vec{e}_z\}dS;$$
$$\varrho(\vec{r},t) = e\sum_k\delta(\vec{r}-\vec{r}^k), \qquad \vec{j}(\vec{r},t) = e\sum_k\vec{v}^k\delta(\vec{r}-\vec{r}^k).$$

Here e and c are the electron charge and speed of light, respectively; $\vec{e}_z$ is the unit vector along the z axis; $\vec{r}^k(t) = \vec{r}(t, t_e^k)$ and $\vec{v}^k(t) = \vec{v}(t, t_e^k)$ are the coordinates and velocity of a k's electron, which entered the interaction region at the moment of time t_e^k ($\vec{v} = d\vec{r}/dt$). For nonrelativistic beams only the potential part [given under the Coulomb gauge ($\vec{\nabla}\cdot\vec{A} = 0$) by the scalar potential φ] of the nonradiated (space-charge) field is usually taken into account, but in a more generic situation one is also bound to include its rotational part (given by the vector potential $\vec{A}^{qs}$) as it could significantly influence the bunching of the electron beam (see, e.g., [20,21]). For the purposes of current analysis the rotational part, $c^{-1}\partial\vec{A}^{qs}/\partial t$, of the nonradiated quasistatic electric field and nonradiated quasistatic magnetic field, $\vec{\nabla}\times\vec{A}^{qs}$, are calculated out of Eqs. (2) [22]. It

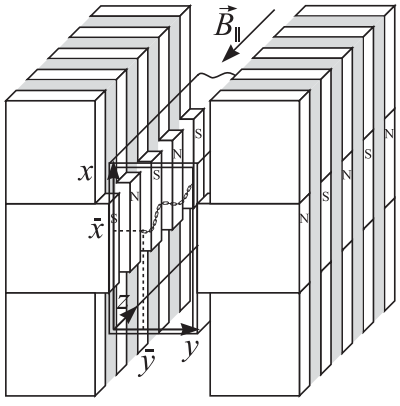

FIG. 1. Schematic drawing of a rectangular waveguide with a mounted permanent magnet planar undulator immersed in the uniform longitudinal (guide) magnetic field.

should be emphasized that the quasistatic vector potential $\vec{A}^{qs}(\vec{r}, t)$ and the amplitude $C(z)$ of synchronous mode depend on the rotational part of the current density $\vec{j}^{r}(\vec{r}, t)$, [22,23].

Thus, by averaging on the electrons' entrance phase, one can reduce the problem of interaction of electron beam with a seed synchronous microwave of frequency ω to the task of solving single-particle equations of motion for arbitrary entrance time t_e and Maxwell's equations in the form of (modified by space-charge inclusion) Kisunko-Vainshtein's equations of excitation for regular waveguides [24,25]. It is exactly in this manner (neglecting all space-charge effects) a highly successful theory of the gyrotron was initially developed by Gaponov [26].

For the amplifier regime we write single-particle equations of motion taking as independent variables the coordinate z and time of entrance of electrons to the interaction region t_e [the time of arrival $t = t(z, t_e)$ of electrons, which entered the interaction region at the time t_e, to the cross section z becomes a dependent variable] in the form

$$\frac{d\vec{p}}{dz} = e\left[\vec{E} + \frac{\vec{p}}{m_e c\gamma} \times (\vec{B}_p + \vec{B})\right]\frac{dt}{dz}, \qquad \frac{dt}{dz} = \frac{m_e\gamma}{p_z}, \qquad \frac{d\vec{r}_\perp}{dz} = \frac{\vec{p}_\perp}{p_z}, \tag{3}$$

where $\vec{E}(\vec{r}_\perp, z, t)$, $\vec{B}(\vec{r}_\perp, z, t)$, and $\vec{B}_p(\vec{r}_\perp, z)$ are given by (1) and (4), respectively; m_e is the electron rest mass; it is also more convenient for numerical calculations to introduce the momentum of an electron $\vec{p} = m_e\vec{v}\gamma$ instead of its velocity $\{\vec{p}_\perp = (p_x, p_y),\ \gamma = [1 + \vec{p}^2/(m_e^2c^2)]^{1/2}\}$. The initial conditions then are $x(z = 0, t_e) = \bar{x}$, $y(z = 0, t_e) = \bar{y}$, $t(z = 0, t_e) = t_e$, $\vec{p}(z = 0, t_e) = m_e(0, 0, V_\parallel)\gamma_0$ $[\gamma_0 = (1 - V_\parallel^2/c^2)^{-1/2}]$ and $C(z = 0) = C_0$. In order to complete the formulation, we use the charge conservation law [27], p. 31, and the fact that in the stationary regime electrons, which enter the interaction region at the time t_e separated by an integral multiple of the period of the amplified microwave, go along identical trajectories (see also [28]). In the discrete model of electron beam we assume that over the period of the amplified microwave macroparticles enter to the interaction region in regular time intervals $2\pi/(\omega N)$; hence, the numerical finding of a solution to the nonlinear self-consistent system (1)–(4) consists in the simultaneous solving of $6(N + 1)$ first-order nonlinear ordinary differential equations.

Magnetostatic field $\vec{B}_p(\vec{r})$ consists of a guide (uniform longitudinal) magnetic field $\vec{B}_\parallel$ and planar spatially periodic undulator magnetic field [12,29]:

$$\vec{B}_p(\vec{r}) = \left[0, -\tilde{B}_\perp \cosh\left(\frac{\pi[2y - b']}{\lambda_w}\right)\sin\left(\frac{2\pi z}{\lambda_w}\right), - \tilde{B}_\perp \sinh\left(\frac{\pi[2y - b']}{\lambda_w}\right)\cos\left(\frac{2\pi z}{\lambda_w}\right) - B_\parallel\right]. \tag{4}$$

where b' is the undulator gap width. Following [28], we model the injection of the electron beam into the interaction region by allowing the undulator amplitude to increase adiabatically from zero to a constant level over N_w undulator periods ($B_\perp = \text{const}$):

$$\tilde{B}_\perp(z) = \begin{cases} B_\perp \sin^2\left(\frac{\pi z}{2\lambda_w N_w}\right), & 0 \le z < N_w\lambda_w, \\ B_\perp, & N_w\lambda_w \le z. \end{cases}$$

III. MAGNETOSTATIC RESONANCE: ENERGY TRANSFER AND DYNAMICAL CHAOS

Having the primary goal in the demonstration of underlying physics, in this section we examine analytically dynamics of an individual test electron only in the magnetostatic field of hybrid planar FEM intentionally considering a simplest possible model of a hybrid planar FEM (which accounts for the undulator through only one component of its spatially periodic magnetic field taken in the limit $2\pi[y - b'/2]/\lambda_w \ll 1$ and neglecting the adiabatic entrance section): $\vec{B}_p = [0, -B_\perp \sin(2\pi z/\lambda_w), -B_\parallel]$.

In components the single-particle equations of motion can be written as

$$\ddot{x}_0 - \omega_\parallel\dot{y}_0 = -\omega_\perp\dot{z}_0 \sin(\omega_0 z_0/V_\parallel), \qquad \ddot{y}_0 + \omega_\parallel\dot{x}_0 = 0, \qquad \ddot{z}_0 = \omega_\perp\dot{x}_0 \sin(\omega_0 z_0/V_\parallel), \tag{5}$$

where (to distinguish from the self-consistent formulation of the previous and subsequent sections) $\vec{r}_0 = (x_0, y_0, z_0)$ denotes the electron coordinates ($\vec{v}_0 = d\vec{r}_0/dt$); $\omega_0 = 2\pi V_\parallel/\lambda_w$ and $\omega_\parallel = |e|B_\parallel/(m_e c\gamma_0)$ are the partial undulator and cyclotron frequencies, respectively; $\omega_\perp = |e|B_\perp/(m_e c\gamma_0)$; the overdots denote differentiation with respect to the transit time t. Properties of solutions to Eqs. (5) are fundamental to the consideration of microwave amplification and generation in an FEM [6,30,31]. It should be noted that out of four quantities λ_w, $B_\perp$, $B_\parallel$, $V_\parallel$ only two of their dimensionless combinations $\varepsilon = \omega_\perp/\omega_0 \equiv c\mathcal{K}/(\gamma_0 V_\parallel)$ ($\mathcal{K}$ is the conventional undulator parameter) and $\sigma_0 = \omega_\parallel/\omega_0$ define the behavior of nonlinear dynamical system (5).

One can easily find a noninvolutive set of three functionally independent first integrals [17] of this nonlinear dynamical system just by integrating its first two equations and taking the energy conservation law as the third linearly independent one:

$$F_1 = P_x - m_e\gamma_0\omega_\parallel y_0, \qquad F_2 = P_y, \qquad F_3 = m_e c^2\gamma_0,$$

where $P_x = m_e\gamma_0[\dot{x}_0 - (2\pi)^{-1}\omega_\perp\lambda_w \cos(\omega_0 z_0/V_\parallel)]$, $P_y = m_e\gamma_0[\dot{y}_0 + \omega_\parallel x_0]$, and $P_z = m_e\gamma_0\dot{z}_0$ are the components of canonical momentum. The Poisson brackets of the first integrals read

$$\{F_1, F_2\} = -m_e\gamma_0\omega_\parallel, \qquad \{F_1, F_3\} = \{F_2, F_3\} = 0,$$

which means that the dynamical system (5) does not fall

under the conditions of the Liouville theorem (cf. [32]). The first integrals are independent if the functional determinant does not vanish (see, e.g., [33]):

$$\frac{\partial(F_1, F_2, F_3)}{\partial(P_x, P_y, P_z)} = \frac{c^2 P_z}{F_3} \neq 0.$$

Therefore, independence of the first integrals is lost and the dimensions of dynamical system are raised whenever $P_z = 0$. The numerical simulations show that all electron trajectories, which satisfy the condition $\dot{z}_0(t) = 0$, are unstable. Below we will use this condition to find an analytical characterization of the onset of dynamical chaos.

System (5) cannot be integrated in quadratures everywhere because it possesses nonzero Lyapunov exponents (see [17] and Fig. 6 below). In the zone of regular dynamics, a solution to system (5) can be obtained by the use of a method of Lindshtedt [34,35] of asymptotic expansion of trajectory and frequencies in the small parameter ε (see [19] for a detailed exposition of the method). To the order $o(\varepsilon^3)$, the velocity components read

$$\begin{aligned}
\dot{x}_0(\tilde{t}) &= \bar{v}_\parallel \frac{\omega_\perp \Omega_0}{\Omega_0^2 - \Omega_\parallel^2}[\cos(\Omega_0 \tilde{t}) - \cos(\Omega_\parallel \tilde{t})], \\
\dot{y}_0(\tilde{t}) &= \bar{v}_\parallel \frac{\omega_\perp \Omega_0}{\Omega_0^2 - \Omega_\parallel^2}\left[\sin(\Omega_\parallel \tilde{t}) - \frac{\Omega_\parallel}{\Omega_0}\sin(\Omega_0 \tilde{t})\right], \\
\dot{z}_0(\tilde{t}) &= \bar{v}_\parallel\left\{1 + \frac{\omega_\perp^2 \Omega_0}{2(\Omega_0^2 - \Omega_\parallel^2)}\left[\frac{\cos([\Omega_0 - \Omega_\parallel]\tilde{t})}{\Omega_0 - \Omega_\parallel}\right.\right. \\
&\quad \left.\left. + \frac{\cos([\Omega_0 + \Omega_\parallel]\tilde{t})}{\Omega_0 + \Omega_\parallel} - \frac{\cos(2\Omega_0 \tilde{t})}{2\Omega_0}\right]\right\},
\end{aligned} \tag{6}$$

where $\bar{v}_\parallel = \kappa V_\parallel$, $\Omega_0 = \kappa\omega_0$, and $\Omega_\parallel = \sigma\omega_\parallel/\sigma_0$; $\tilde{t} = t - t_e$ is the electron transit time. Here κ and σ to the order $o(\varepsilon^3)$ are given as functions of ε and σ_0 by the following "self-consistent" system of algebraic equations:

$$\kappa = 1 - \frac{\varepsilon^2(3\kappa^2 + \sigma^2)}{4(\kappa^2 - \sigma^2)^2}, \qquad \frac{\sigma}{\sigma_0} = 1 + \frac{\varepsilon^2(\kappa^2 + \sigma^2)}{4(\kappa^2 - \sigma^2)^2}. \tag{7}$$

An analytical solution to Eqs. (7) can be found by successive iterations starting with "nonrenormalized" values 1 and σ_0 for κ and σ, respectively. It is worth noting that Eqs. (7) order by order in ε provide cancellation of secular terms in the solution procedure for system (5). Using Eqs. (6) and (7), one can check that $\tilde{v}_0^2$ is conserved to the order $o(\varepsilon^3)$ and is equal to $V_\parallel^2$ as required by the conservative nature of system (5). It should be also noted that this solution to the order $o(\varepsilon^3)$ is valid not only under assumptions made at the beginning of this section but also for its "realizable" counterpart (4) (if $\tilde{B}_\perp$ holds constant). The trajectories of electrons are then given by a straightforward integration.

From (6) it follows that the motion of an individual test electron is a superposition of constant motion with velocity $\bar{v}_\parallel$ and three-dimensional oscillations with normal undulator Ω_0 and cyclotron $\Omega_\parallel$ frequencies, which differ from their partial analogues ω_0 and $\omega_\parallel$ by "renormalization" multipliers κ and σ/σ_0. Recall that each subsystem of a nonlinear dynamical system possesses its own (partial) oscillation frequency if interaction between subsystems vanishes. Nonzero interaction modifies those oscillation frequencies by some amount [36] (represented here by multipliers κ and σ/σ_0); κ also shows what portion of electron initial kinetic energy is transferred to the constant motion. As $\Omega_\parallel$ tends to Ω_0 the amplitudes of transversal and longitudinal oscillations increase. This signifies the existence of an internal resonance [37], i.e., a resonant transfer of kinetic energy from longitudinal constant motion to transversal and longitudinal oscillatory degrees of freedom. We call this situation magnetostatic resonance or *magnetoresonance* as is customary in the FEM theory [38].

Calculation of normal undulator and cyclotron frequencies Ω_0 and $\Omega_\parallel$ requires solution for κ and σ of the system of two algebraic equations (7). To achieve maximal accuracy it turns out advantageous to solve this system numerically and use thus obtained values of κ and σ in the analytical calculations. In Fig. 2 the results of such a solution are shown (black and red solid lines). For comparison, the result of calculation of κ and σ via Fourier analysis of direct numerical solution of Eqs. (5) for the velocity components is also given (shown by dots in Fig. 2). In Fig. 3 the graphs of κ and σ vs $B_\parallel$ are shown in more detail for the guide magnetic field values around the magnetoresonance. At the magnetoresonance $B_\parallel^{\text{res}} \approx 6.67$ kG the normal frequencies Ω_0 and $\Omega_\parallel$ experience jumps in order to comply with the conservation of kinetic energy in the dynamical system (5). As ε grows above a certain threshold value, two zones of regular dynamics become separated by a chaotic zone centered about the

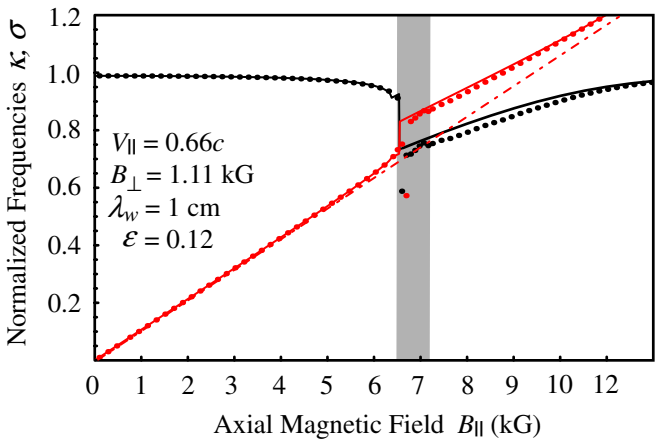

FIG. 2. (Color) κ and σ as functions of the guide magnetic field $B_\parallel$. κ and σ are depicted in black and red colors, respectively; for reference $\sigma_0(B_\parallel)$ is given by the dashed line. The shaded area corresponds to the zone of chaotic dynamics as given by the criterium (8).

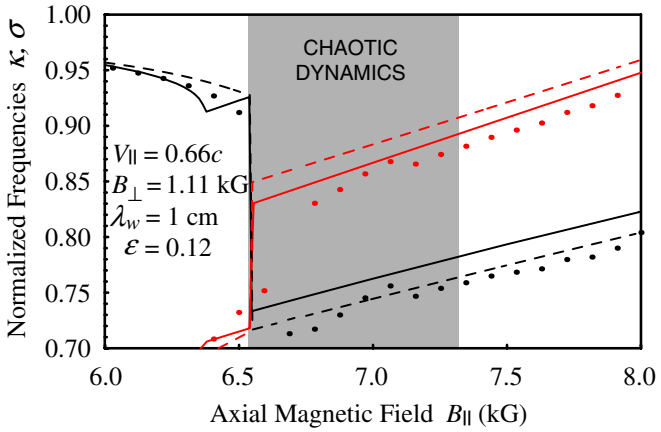

FIG. 3. (Color) κ and σ as functions of the guide magnetic field for $B_\parallel$ values around the magnetoresonance. κ and σ are depicted in black and red colors, respectively; for reference $\sigma_0(B_\parallel)$ is given by the dashed line.

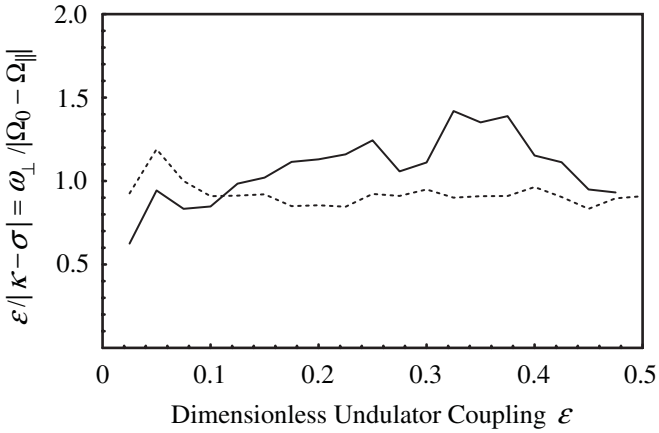

FIG. 4. Maximal value of magnetoresonant multiplier as a function of dimensionless coupling ε.

magnetoresonant value of the guide magnetic field (see Fig. 3).

Mutual orientation of the undulator and guide magnetic fields causes the kinetic energy transfer from the longitudinal constant motion to undulator vibrational (frequencies ω_0 and Ω_0) and then to cyclotron vibrational (frequencies $\omega_\parallel$ and $\Omega_\parallel$) degrees of freedom of the nonlinear dynamical system (5); the coupling is provided by the amplitude of undulator magnetic field $B_\perp$ ($\varepsilon = \omega_\perp/\omega_0$). Such a picture allows one two possible ways of energy transfer: at magnetoresonant ($\Omega_0 \approx \Omega_\parallel$) and nonmagnetoresonant ($\Omega_0 \not\approx \Omega_\parallel$) coupling regimes. Obviously, the magnetoresonant regime requires smaller coupling and may become more advantageous for microwave FEM amplifiers and oscillators. It is then necessary to clarify how accessible these regimes are of FEM operation.

Characterizing the onset of chaos by condition $\dot{z}_0(t) = 0$, we propose the following estimate for the range of parameters corresponding to the chaotic dynamics:

$$|\Omega_0 - \Omega_\parallel| < \omega_\perp \quad (|\kappa - \sigma| < \varepsilon). \tag{8}$$

This analytical estimate is confirmed by numerical calculations and is consistent with Chirikov resonance-overlap criterium [39], i.e., appearance of the chaotic state takes place whenever the difference between normal frequencies of the system becomes less than the coupling. As will be shown in Sec. IV, the absolute value of the ratio $\omega_\perp/(\Omega_0 - \Omega_\parallel)$ (called below the *magnetoresonant multiplier*) defines the microwave gain. Results of numerical calculations of its maximal value for zones of regular dynamics and practically accessible $\varepsilon(B_\perp, V_\parallel)$ are given in Fig. 4 (for each value one needs to optimize $B_\parallel$; solid and dotted lines correspond to the approach of the chaotic zone from low and high values of the guide magnetic field, respectively). This shows that in the magnetoresonant case there exists limitation on the fraction of energy transferred from constant motion to oscillatory (transversal and longitudinal) degrees of freedom posing a fundamental limit on an FEM efficiency. A calculation shows that $\overline{\dot{x}_0^2(\tilde{t}) + \dot{y}_0^2(\tilde{t})}/\overline{\dot{z}_0^2(\tilde{t})} \approx 0.48$ (bars denote time averaging). In Fig. 5 we present a contour plot of $\kappa \equiv \bar{v}_\parallel/V_\parallel$ as a function of dimensionless coupling ε and guide magnetic field σ_0. The region of chaotic dynamics is given in black. In Fig. 6 a map of the major Lyapunov exponent as a function of ε and σ_0 is shown. The calculation included a check that the sum of all Lyapunov exponents is equal to zero as mandatory for a conservative dynamical system because of the Liouville theorem.

It should be noted that in general the presence of nonzero initial transversal velocity $V_\perp = (V_x^2 + V_y^2)^{1/2}$ influ-

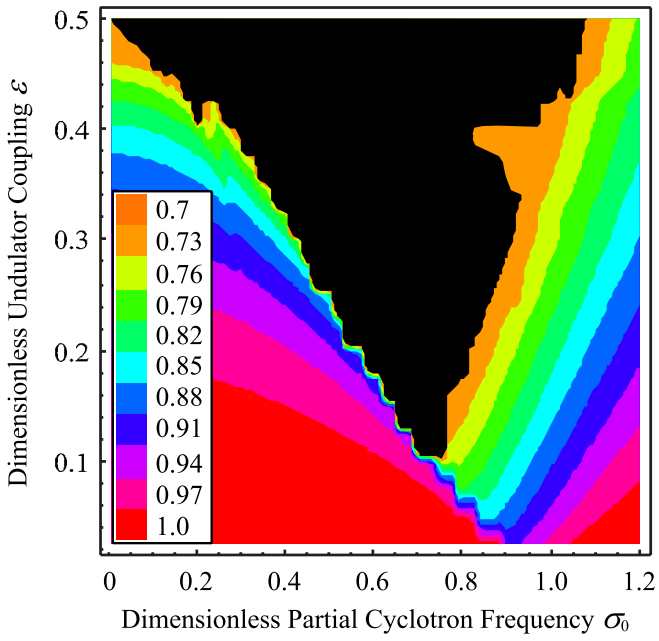

FIG. 5. (Color) Contour plot of $\kappa \equiv \bar{v}_\parallel/V_\parallel$ as a function of dimensionless coupling ε and guide magnetic field σ_0. The region of chaotic dynamics is given in black.

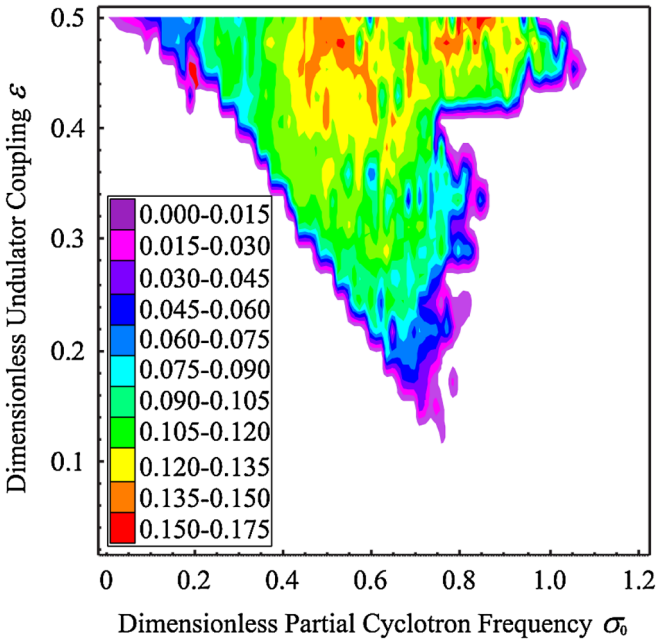

FIG. 6. (Color) Map of the major Lyapunov exponent.

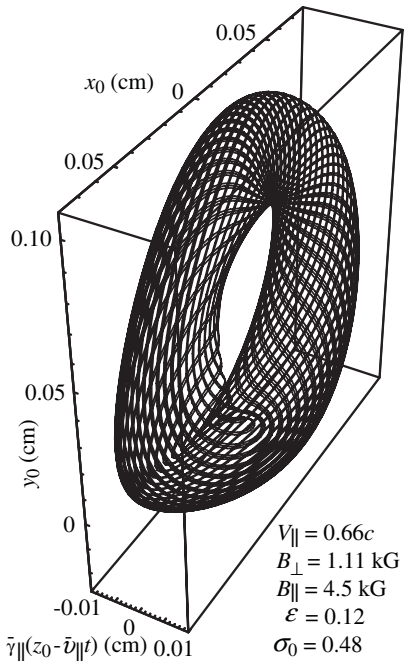

FIG. 7. Electron trajectory (winding of two-dimensional torus) under conditions of regular dynamics.

ences the shape of the chaotic dynamics zone. A calculation similar to that in the case $V_x = V_y = 0$ shows that the influence of V_y is symmetric regarding its sign and, hence, is less relevant while that of V_x is much more important. In particular, the x component of the initial velocity of a certain sign can either suppress ($V_x > 0$) or enhance ($V_x < 0$) the zone of chaotic dynamics. Nonzero V_x also changes the position of the edge of the regular dynamics zone at the zero guide magnetic field. This is due to the fact that the position of the separatrix on the phase plane z_0-$\dot{z}_0$ depends on the value and sign of V_x and is independent of V_y. The position of the edge of the chaotic zone at zero guide magnetic field ($\sigma_0 = 0$) is calculated to be $\varepsilon = \{[1 + (V_x/V_\parallel)^2]^{1/2} + V_x/V_\parallel\}/2$.

Finally, let us emphasize two important points about the nonlinear conservative dynamical system (5). First, the use of a method of Lindshtedt for finding electron trajectories allows one to achieve cancellation of nonphysical secular terms in the series expressions. Second, the system is degenerate in the sense that at zero amplitude of the undulator magnetic field or the zero guide magnetic field, the dynamics is characterized by only one normal frequency instead of two. Under such conditions (after subtraction of constant motion along the z axis), electron trajectories constitute invariant curves, while in the generic case solutions (6) strongly indicate that they wind up (surfaces diffeomorphic to) two-dimensional invariant tori. Under natural projection into the system's configuration space (cf. [33], p. 192), one can visualize such a two-dimensional torus (Fig. 7) in the reference frame, which moves with the mean velocity $\bar{v}_\parallel$ of electron, $\bar{\gamma}_\parallel = (1 - \bar{v}_\parallel^2/c^2)^{-1/2}$. This regular behavior is exhibited by the dynamical system under investigation only for the particular range of dimensionless parameters ε and σ_0 (cf. [40]) as can be understood from Fig. 5. When parameters change in such a way that the motion of electrons becomes chaotic, we can observe the disintegration of the corresponding invariant torus shown in Figs. 8 and 9. In Fig. 8 the

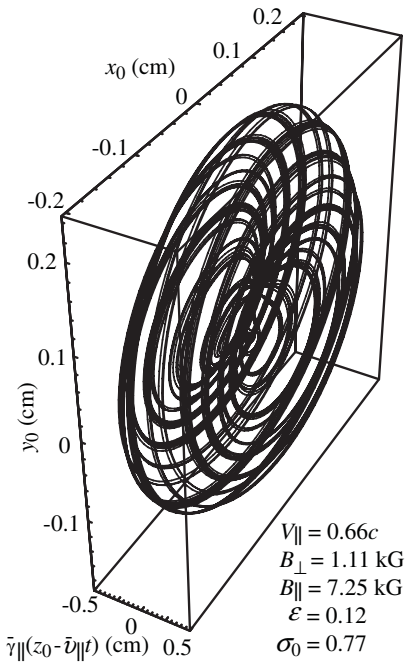

FIG. 8. Disintegration of an invariant torus for a short period of time.

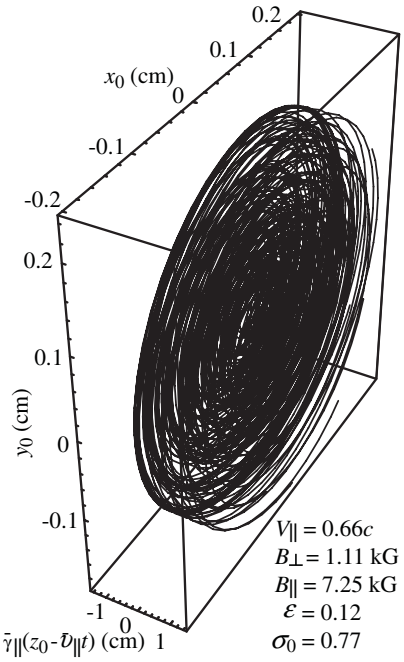

FIG. 9. Disintegration of an invariant torus for a long period of time.

trajectory of the electron is drawn for a small period of time and looks like winding up a two-dimensional torus, while for a longer period of time it does not (Fig. 9).

Summarizing this section, we observe that there are two regimes for pumping kinetic energy into transversal degrees of freedom of a hybrid planar FEM: the first one (advocated here as a more efficient one for the terahertz waveband) consists in low amplitude of undulator magnetic field and the guide magnetic field as close to its magnetoresonant value as only consistent with the regular dynamics; the second regime (usually considered in the literature) would also provide the same ratio $\omega_\perp/(\Omega_0 - \Omega_\parallel)$ through a high absolute value of $|\Omega_0 - \Omega_\parallel|$ given by an off-resonant guide magnetic field $B_\parallel$ and a necessarily high value of amplitude of the undulator magnetic field $B_\perp$. It, however, seems that values of $B_\perp$ in excess of 10 kG are currently practically unattainable while guide magnetic fields of up to 50 kG can be presently achieved.

IV. LINEAR AMPLIFICATION: MAGNETOSTATIC RESONANCE AND MAXIMAL GAIN

Knowledge of electrons' trajectories (6) in the (ideal) magnetostatic field of hybrid planar FEM allows one to develop a gyrotronlike analytical linear theory of microwave amplification. In particular, in Ref. [41] such an approach was constructed for interaction of an electron beam with a mode of an arbitrary regular waveguide in a hybrid FEM as a perturbation theory in the microwave fields $\vec{E}$ and $\vec{B}$ ($B_\parallel$, $B_\perp \gg c|\vec{E}|/|\vec{v}|$, $|\vec{B}|$). It is based on the representation of electron trajectory as

$$\vec{r}(t, t_e) \equiv \vec{r}(\tilde{t}, t_e) = \vec{r}_0(\tilde{t}) + \mathrm{Re}\{\vec{r}_1(\tilde{t})e^{i\omega t_e}\} \quad (|\vec{r}_0| \gg |\vec{r}_1|).$$

It should be noted that an analytical theory of this type is valid not only far away from the magnetoresonance ($\Omega_0 \approx \Omega_\parallel$, cf. [42]) but also in its close vicinity. Here we will apply this theory to study amplification of microwaves in a hybrid planar FEM under conditions of magnetoresonance using as an example amplification of TE_{10} and TE_{01} modes of rectangular waveguide with wide a and narrow b sides. The operation at the TE_{10} and TE_{01} modes allows one to utilize the advantage of the enhanced current of sheet electron beams [cf., for example, (11)]. Specifically, neglecting the space charge we need to solve, linearized in the microwave field, a coupled system of equations of excitation (1) and motion (3) given by a system of ordinary differential equations with quasiperiodic coefficients. Its exact solution is achieved by application of a quasiperiodic analogue of Floquet's theorem and, under some additional conditions, comes in the form of an infinite series in undulator and cyclotron harmonics [43], pp. 90–96. Under particular synchronism conditions the series may be truncated to retain a solution pertinent to this very synchronism neglecting other combination ones (see [25,26]). In this case, we can write $C(z) = C_0 \exp(i\delta k_z z)$ for the microwave amplitude ($|\delta k_z| \ll |k_z^0|$), where δk_z is the spatial growth rate.

Under the condition of undulator synchronism

$$\omega - k_z^0 \bar{v}_\parallel \approx \Omega_0, \tag{9}$$

we obtain dispersion equations:

$$\delta k_z\left(\delta k_z - \frac{\delta\omega}{\bar{v}_\parallel}\right)^2 = \mp \frac{\pi|I_0|}{2c\bar{U}\gamma_0^3} \frac{\omega_\perp^2}{(\Omega_0^2 - \Omega_\parallel^2)^2} \times \begin{cases} \frac{\Omega_\parallel^2 \omega}{abc}\sin^2(\frac{\pi\bar{x}}{a}), & \mathrm{TE}_{10}\ \mathrm{mode}\,\{k_z^0 = [(\omega/c)^2 - (\pi/a)^2]^{1/2}\}; \\ \frac{\Omega_0^2 \omega}{abc}\sin^2(\frac{\pi\bar{y}}{b}), & \mathrm{TE}_{01}\ \mathrm{mode}\,\{k_z^0 = [(\omega/c)^2 - (\pi/b)^2]^{1/2}\}; \end{cases} \tag{10}$$

where $\bar{U} = m_e\bar{v}_\parallel^2/(2|e|)$ is the nonrelativistic beam voltage of constant motion and $\delta\omega = \omega - k_z^0\bar{v}_\parallel - \Omega_0$ is a small mismatch from the ideal synchronism ($\delta\omega = 0$). The conditions for existence of two complex conjugated roots of each of Eqs. (10) consist in positivity of their respective cubic discriminants. These yield in each case the thresholds for such instabilities to occur [44]. Similar to the conclusions in Ref. [45], we find that interaction between the transverse component of oscillatory motion and microwave results primarily in axial bunching, which becomes the main source of instability. Nevertheless (unlike in [45]), this comes from analytical expressions, which are valid for all regular dynamics parameters as found in Sec. III and, specifically, near the magnetoresonance.

For the ideal synchronism ($\delta\omega = 0$) the spatial growth rate of the TE_{10} mode is given by

$$\mathrm{Im}\,\delta k_z = \frac{\sqrt{3}}{2\gamma_0}\left(\frac{\pi\omega|I_0|}{2abc^2\bar{U}}\right)^{1/3}\left(\frac{\omega_\perp\Omega_\parallel}{\Omega_0^2-\Omega_\parallel^2}\right)^{2/3}\sin^{2/3}\left(\frac{\pi\bar{x}}{a}\right). \tag{11}$$

$\mathrm{Re}\delta k_z$ provides a correction to the cold propagation constant, k_z^0, caused by the presence of electron beam. Result (11) is similar to those found previously (cf., e.g. [46]) and also implies that there could exist a substantial enhancement in the (microwave) gain, $G = 8.63\,\mathrm{Im}\delta k_z$, because of the presence of a guide magnetic field. It is also significant that *analytical* expression (11) provides a close approximation of the growth rate, which is in good agreement with the numerical simulations of the nonlinear self-consistent system of relativistic equations of motion and equation of excitation. This is mainly due to the fact that in Ω_0 and $\Omega_\parallel$ we account for the initial electron velocity and magnitudes of magnetostatic fields not only through the definitions of ω_0 and $\omega_\parallel$ but also via "renormalization" multipliers κ and σ [cf. (7) and Fig. 2].

More importantly, utilizing results obtained in Sec. III, we can provide an analytical estimate for the maximal attainable gain. To accomplish this task, let us substitute from (8) to find

$$\omega_\perp\Omega_\parallel/(\Omega_0^2-\Omega_\parallel^2) < \Omega_\parallel/(\Omega_0+\Omega_\parallel). \tag{12}$$

Recall that there exists two ways of having the value of magnetoresonant multiplier, $\omega_\perp/(\Omega_0-\Omega_\parallel)$, close to 1: one should either work far from the magnetoresonance (and provide for a strong undulator amplitude $B_\perp$) or, as advocated at the end of Sec. III, operate near the magnetoresonance $\Omega_0 \approx \Omega_\parallel$ with a moderate undulator amplitude (see also Fig. 4). From the inspection of the right-hand side of (12), we observe that its value is about $1/2$ around the magnetoresonance. This provides another reason for preferring a hybrid planar FEM operation regime slightly above the magnetoresonance in order to ensure the regular dynamics of electron motion as detailed in Sec. III (see also Figs. 2, 3, and 5). We, therefore, find for the upper limit on the maximal (near) magnetoresonant gain of a hybrid planar FEM under conditions of ideal undulator synchronism ($\delta\omega = 0$):

$$G_{\max}^{\mathrm{res}} \approx \frac{3.7}{\gamma_0}\left(\frac{\pi\omega|I_0|}{abc^2\bar{U}}\right)^{1/3}\sin^{2/3}\left(\frac{\pi\bar{x}}{a}\right). \tag{13}$$

The same conditions of regular dynamics (8) lead to an important result that around the magnetoresonance the maximal gain is independent of $B_\perp$ (although entering $\bar{v}_\parallel$ in $\bar{U}$ through κ, it cancels out completely by virtue of synchronism condition $[\bar{v}_\parallel = \omega/(k_z^0(\omega) + 2\pi/\lambda_w)]$; as a function of frequency, $G_{\max}^{\mathrm{res}} \sim (k_z^0 + 2\pi/\lambda_w)^{2/3}\bar{\gamma}_\parallel^{-1}\omega^{-1/3}$.

Under the assumption of undulator synchronism in the limit $B_\parallel = 0$ ($\sigma = 0$ and $\kappa \approx 1 - 3\varepsilon^2/4$), an electron beam without initial transverse velocity does not interact with the TE_{m0} modes of a rectangular waveguide. Then the TE_{01} mode turns out to be the lowest one amplified by such an electron beam, and the bottom line of Eqs. (10) can be used to estimate analytically the gain of a planar FEM amplifier without the guide magnetic field (cf. [29])

$$G|_{B_\parallel=0} = \frac{5.93}{\gamma_0}\left(\frac{\pi\omega|I_0|}{abc^2\bar{U}}\right)^{1/3}\left(\frac{\omega_\perp}{\Omega_0}\right)^{2/3}\sin^{2/3}\left(\frac{\pi\bar{y}}{b}\right). \tag{14}$$

Although, it should be noted that magnetoresonant gain $[\Omega_0 \approx \Omega_\parallel$ and $\omega_\perp/(\Omega_0 - \Omega_\parallel) \approx 1]$ calculated using the bottom line of Eqs. (10) is always greater than that one given by Eq. (14).

Another important characteristic of an amplifier is its tunability. In the case of undulator synchronism the frequency tuning of an FEM amplifier is achieved by changing the initial axial velocity, $V_\parallel$, of the electron beam and turns out to be limited only by the requirement of single-mode operation regime. In Fig. 10 for the fundamental TE_{10} mode, one can see that the maximal resonant gain depends weakly on the frequency in the operating range. To provide the single-mode operation regime and interaction only with the forward wave, the frequencies are

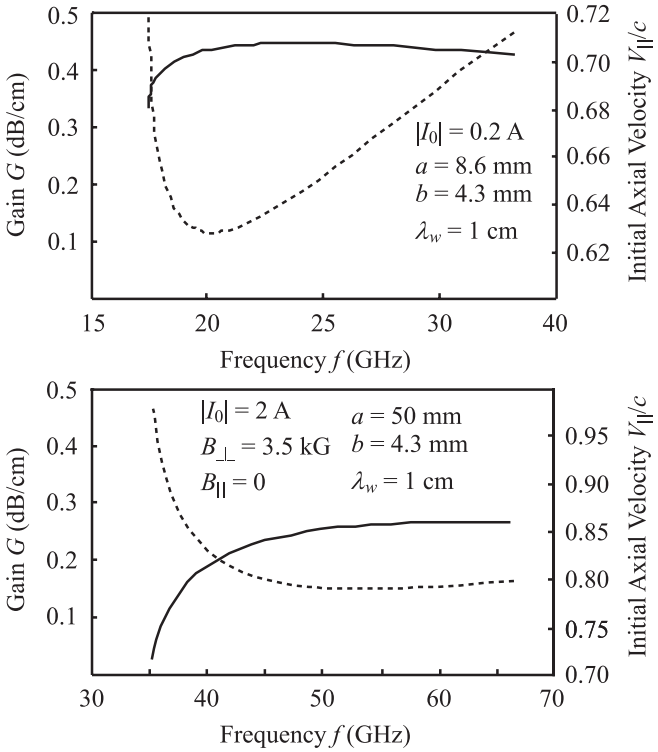

FIG. 10. In the top figure results of analytical calculations of the maximal resonant gain (solid line) and initial axial velocity of the beam (dashed line) for the fundamental TE_{10} mode are presented. In the bottom figure we show the gain (solid line) and initial axial beam velocity (dashed line) at $B_\parallel = 0$ for the TE_{01} mode. All quantities are shown as functions of amplified frequency.

chosen to range from 18 to 32 GHz in this case. Results of gain calculations for interaction with the TE_{01} mode are also shown in Fig. 10. The initial axial velocity must also change with the frequency [$\bar{v}_\parallel = \omega/(k_z^0(\omega) + 2\pi/\lambda_w)$] as shown in both parts of Fig. 10 to maintain the ideal undulator synchronism [in the top figure for calculation of $V_\parallel$ from a given $\bar{v}_\parallel$ we choose $\kappa = 0.8$, see Fig. 5; in the bottom figure to obtain $V_\parallel$ from a given $\bar{v}_\parallel$ one needs to solve the equation $\bar{v}_\parallel = \kappa(V_\parallel)V_\parallel$, see (7) and note that in this case $\sigma = 0$].

V. NONLINEAR SIMULATIONS OF MICROWAVE AMPLIFICATION

Numerical simulations of FEM characteristics are usually concerned with those, as a rule integral, quantities, which can be directly measured experimentally (e.g. saturation power, efficiency, start current, etc.). However, a substantial advantage of numerical calculations also lies in the opportunity of detailed reconstruction of electrons dynamics and their interaction with the microwave field in an FEM. Note also that experimental setups of hybrid planar FEMs under development are supposed to operate far from the magnetoresonance, but such regimes are not optimal in terms of efficiency of microwave amplification because of weak effective pumping of electron oscillations. As found in Sec. IV, the optimal amplification is achieved near the magnetoresonance $\Omega_0 \approx \Omega_\parallel$. This operational regime of a hybrid planar FEM is studied in the literature analytically and numerically in comparatively less detail, mainly, inasmuch as the major attention of researches has been devoted to hybrid helix and coaxial FEM schemes. For example, in the hybrid helix scheme, one uses an annular electron beam, which adiabatic entrance is incompatible with the magnetoresonant condition [45] since the electrons entering the interaction region with different radial separations from the symmetry axis of the undulator magnetic field experience large gradients of the undulator magnetic field, reach orbits characterized by a substantial mean velocity spread (this orbits fail to be the desired stationary helicoidal ones), and do not provide an adequate amplification of microwaves. In the planar FEM on the undulator synchronism this drawback is offset substantially because a sheet electron beam enters in the symmetry plane of the undulator magnetic field and, therefore, can efficiently amplify microwaves under the magnetoresonant condition.

In numerical simulations of this section, expression (4) is used for the magnetostatic field of hybrid planar FEM, i.e., not only do we allow for the transverse inhomogeneity of undulator magnetic field but also take into account the adiabatic entrance section (with $N_w = 6$).

According to the analytical results of Sec. IV, the predominant phasing mechanism on the undulator synchronism is the axial one. A numerical verification to this fact is provided in the top of Fig. 11 [calculation of bunching is performed neglecting the nonradiated (space-charge) field of electron beam]. The black dashed curve in the bottom of Fig. 11 is also calculated neglecting the space-charge field. The blue dash-dotted curve gives the microwave power, $P(z) = |C(z)|^2 P_0$, if only the potential part, $-\vec{\nabla}\varphi$, of the space-charge field [see Eqs. (1) and (2) in Sec. II] is taken into account. The red solid curve is obtained when both the potential and rotational (given by the vector potential $\vec{A}^{qs}$) parts of the space-charge field are included in the calculations. In the region 1 bunches are created in the uniform at the entrance ($z = 0$) electron beam under the influence of the seed microwave in its decelerating phase. The interaction of the electron beam with the microwave is almost linear and the microwave power $P(z) = |C(z)|^2 P_0$ grows exponentially with $2\,\mathrm{Im}\delta k_z = 0.027\ \mathrm{cm}^{-1}$. In region 2, the electron beam is maximally bunched and efficiently amplifies the microwave (simultaneously about $0.35N$ of the beam electrons, which entered the interaction region at $z = 0$ in the accelerating phase of the microwave, draw the power from the microwave); the total microwave power in this region increases almost linearly. In region 3, the en-

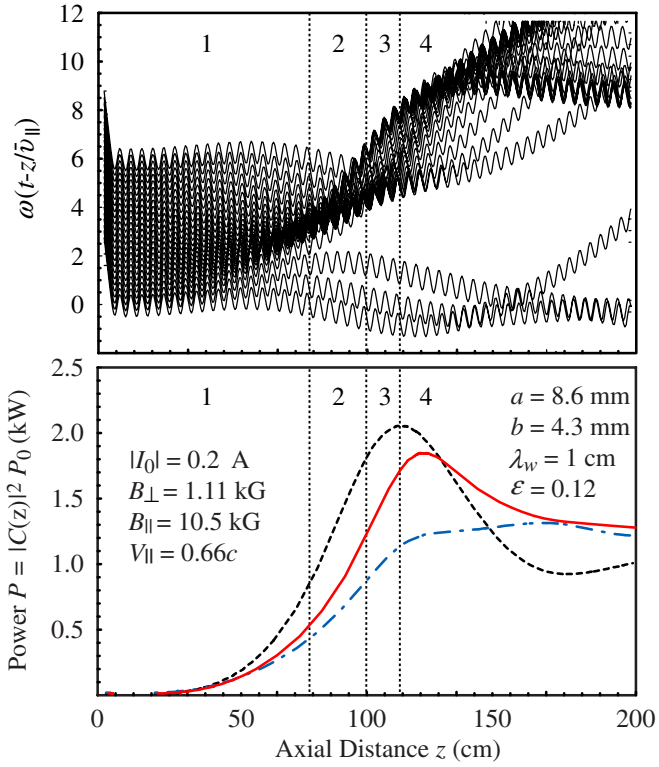

FIG. 11. (Color) Results of numerical calculations of electron beam bunching and microwave power amplification (assumed current density 0.5 A/mm^2). The black dashed curve is calculated neglecting the space-charge field; the blue dash-dotted curve gives the microwave power if only the potential part of the space-charge field [see Eqs. (1) and (2) in Sec. II] is taken into account; the red solid curve is obtained when both the potential and rotational (given by the vector potential $\vec{A}^{qs}$) parts of the space-charge field are included in the calculations.

ergy flow from the electrons, which amplify the microwave, and those that draw microwave power reaches the balance and the microwave power attains saturation. In region 4, there occurs the second (like region 2) consolidation of bunches at $z = 135$ cm, which subsequently leads to the second maximum of microwave power at $z = 230$ cm, and so on. It is also worth noting that electrons, which entered the interaction region at $z = 0$ in the accelerating phase of the microwave, are weaker trapped than those entering the interaction region at $z = 0$ in the decelerating phase. The small-amplitude fast vibrations in the top of Fig. 11 are caused by the oscillations of longitudinal velocity of electrons around its mean value $\bar{v}_\parallel$ [see (6)]. A simple analytical consideration illustrates the contribution of the rotational part of space-charge field. For the predominantly axial nature of bunching at the undulator synchronism as discussed above (see also [28]), we may take into account only the axial component of the current density and can show that $A_z^{qs} \approx (\bar{v}_\parallel/c)\varphi$. Thus, we derive the following approximate relations on an electron's trajectory:

$$E_x^{r|qs} \approx E_y^{r|qs} \approx B_z^{qs} \approx 0, \qquad E_z^{r|qs} \approx -\frac{\bar{v}_\parallel^2}{c^2} E_z^p,$$

$$\frac{e}{c}(\vec{v} \times \vec{B}^{r|qs})_{x,y} \approx -e\frac{\bar{v}_\parallel^2}{c^2} E_{x,y}^p,$$

i.e. the contribution to the Lorentz force from the longitudinal component of the rotational part, $E_z^{r|qs}$ [$\vec{E}^{r|qs} = -\partial\vec{A}^{qs}/(c\partial t)$], of the space-charge electric field has opposite sign to that of its potential part, E_z^p ($\vec{E}^p = -\vec{\nabla}\varphi$), and in the laboratory frame the contribution from the space-charge magnetic field can be expressed through the same potential part of the space-charge electric field. It therefore follows that beyond the nonrelativistic situation the influence of the nonradiated (space-charge) field becomes smaller as $\bar{v}_\parallel$ grows:

$$\vec{F}_L^{qs} = e\left(\vec{E}^p + \vec{E}^{r|qs} + \frac{\vec{v}}{c} \times \vec{B}^{qs}\right) \approx -e\left(1 - \frac{\bar{v}_\parallel^2}{c^2}\right)\vec{\nabla}\varphi.$$

A. Interaction with resonant wave

Results of numerical calculations (neglecting the space-charge fields) of various characteristics of hybrid planar FEM as functions of the guide magnetic field $B_\parallel$ are plotted in Fig. 12. One can see that the optimal amplification frequency (the frequency providing for the maximal growth rate) for undulator synchronism [see (9)] depends on the guide magnetic field since the mean velocity of constant motion, $\bar{v}_\parallel$, is also a function of $B_\parallel$ at least through the "renormalization" multiplier κ. Under the undulator synchronism the gain, G, and efficiency, η,

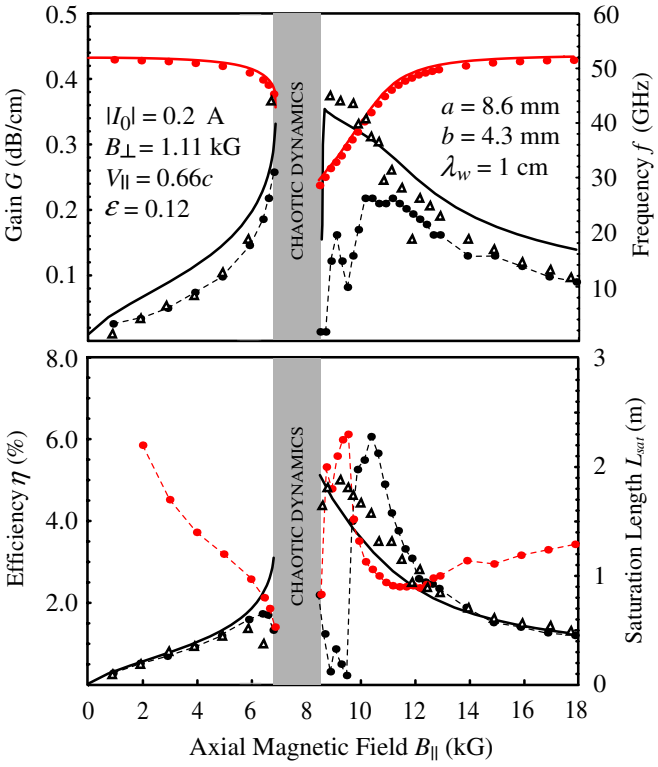

FIG. 12. (Color) In the top figure, solid black (gain G) and red (frequency f) curves are obtained from analytical expressions (9) and (10); the dots of respective colors are results of numerical simulations. In the bottom figure, black (saturation efficiency η) and red (saturation length $L_{\rm sat}$) dots are obtained through numerical simulation; the solid black curves give an analytical order-of-magnitude estimate for the efficiency. Triangles represent results of the calculation of gain and efficiency, respectively, for simplified magnetostatic field of Sec. III. All quantities are calculated as functions of $B_\parallel$ for the TE_{10} mode amplification under the undulator synchronism neglecting the space-charge field of the electron beam. The darkened area corresponds to the chaotic dynamics zone around the magnetoresonance ($B_\parallel^{\rm res} \approx 6.67$ kG).

attain their maximal values ($G \approx 0.23$ dB/cm and $\eta \approx 6.6\%$) for the guide magnetic field ($B_\parallel \sim 10.5$ kG) higher than its magnetoresonant value. An analytical estimate of the width of chaotic dynamics zone for the undulator synchronism gives $B_\parallel \in (6.6, 7.3)$ kG around the magnetoresonance $B_\parallel^{\rm res} \approx 6.67$ kG; numerical simulations exhibit a somewhat wider chaotic dynamics zone. Maximal gain and efficiency for the magnetostatic field (4) are achieved at larger separations from the chaotic dynamics zone than for the simplified magnetostatic field of Sec. III. In a linear theory the efficiency can be evaluated as $\eta = (\gamma_{\max} - \gamma_{\min})/(\gamma_{\max} - 1)$, where $\gamma_{\max}$ and $\gamma_{\min}$ are the maximal and minimal values of the relativistic factor for which the spatial growth rate does not vanish. An analysis of the dispersion equation [see (10)] allows one to obtain the following order-of-magnitude estimate:

$$\eta \approx \frac{\gamma_0^3 V_\parallel^2}{(\gamma_0 - 1)c^2} \frac{3.8 Q^{1/3}}{k_z^0 + 2\pi/\lambda_w},$$

where Q denotes the right-hand side of the dispersion equation [see (10)]. Observe a greater efficiency of microwave amplification for the guide magnetic field greater than its magnetoresonant value since under such conditions a larger portion of the energy of constant longitudinal motion is transferred to the transversal oscillations of electrons.

The influence of the space-charge field of the electron beam is demonstrated in Fig. 13, which shows the saturation efficiency, η, as a function of the guide magnetic field, $B_\parallel$, obtained through direct numerical simulations of Eqs. (1) and (2). The parameters of beam-microwave interaction correspond to those of Fig. 12. The black dashed curve is the same as the black dots representing the saturation efficiency in the bottom of Fig. 12, i.e., it is obtained completely neglecting the space-charge field. The blue dash-dotted curve is calculated taking into account only the potential part, $-\vec{\nabla}\varphi$, of the space-charge field of the electron beam. The red solid curve gives the saturation efficiency when both the potential and rotational (given by the vector potential $\vec{A}^{qs}$) parts of space-charge field are included in the calculations (cf. Fig. 11). As expected from a simple analytical demonstration above, the contribution of the rotational part offsets that of the potential one. It can be seen that, for the guide magnetic field values slightly above the upper edge of chaotic dynamics zone, the influence of the space-charge field on microwave amplification

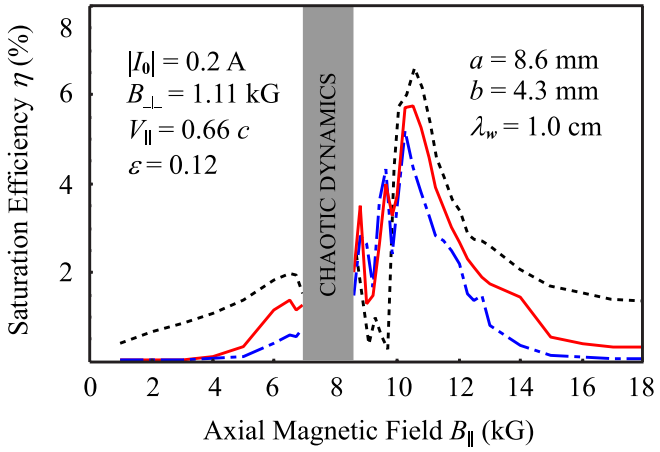

FIG. 13. (Color) The influence of the space-charge field on the saturation efficiency of a hybrid planar FEM at the undulator synchronism (current density 0.5 A/mm^2). The black dashed curve is calculated neglecting the space-charge field; the blue dash-dotted curve gives the microwave power if only the potential part, $-\vec{\nabla}\varphi$, of the space-charge field is taken into account; the red solid curve is obtained when both the potential and rotational (given by the vector potential $\vec{A}^{qs}$) parts of the space-charge field are included in the calculations.

is much less than for its values far away from the magnetoresonance. This circumstance, in our view, has a twofold explanation. First, mean transverse separations between electrons turn out to be almost an order of magnitude higher than for the guide magnetic field values far away from the magnetoresonance. Second, in these conditions, at some regions of interaction space the magnetostatic field of the hybrid planar FEM leads to a more dense longitudinal bunching of the electron beam, thus, enhancing the degree of its grouping.

B. Influence of initial velocity spread

To study the influence of electron beam initial velocity spread on performance of a hybrid planar FEM amplifier, let us assume that the components of initial velocity of electrons, $\vec{v} = (m_e\gamma_0)^{-1}\vec{p}(z = 0, t_e)$, are independent random variables and each of them is characterized by the probability density,

$$w(v_i) = \frac{1}{\sqrt{2\pi}\delta v_i} \exp\left[-\frac{(v_i - \bar{v}_i)^2}{2\delta v_i^2}\right] \quad (i = x, y, z),$$

where $\bar{v}_i$ and δv_i are the means and variances, respectively ($\bar{v}_x = \bar{v}_x = 0$ and $\bar{v}_z = V_\parallel$). To obtain a statistically valid result the saturation efficiency, η, is averaged over realizations of random initial velocities of electrons. The typical dependence of mean saturation efficiency $\bar{\eta} = M^{-1}\sum_{i=1}^{M}\eta_i$ on the realization number M is shown in Fig. 14.

In numerous test runs we found out that the relative mean efficiency calculated with three-dimensional initial velocity spread is equal to the product of relative mean efficiencies computed with one-dimensional spreads only:

$$\frac{\bar{\eta}(\delta v_x, \delta v_y, \delta v_z)}{\eta(0,0,0)} \approx \frac{\bar{\eta}(\delta v_x, 0, 0)}{\eta(0,0,0)} \frac{\bar{\eta}(0, \delta v_y, 0)}{\eta(0,0,0)} \times \frac{\bar{\eta}(0, 0, \delta v_z)}{\eta(0,0,0)}.$$

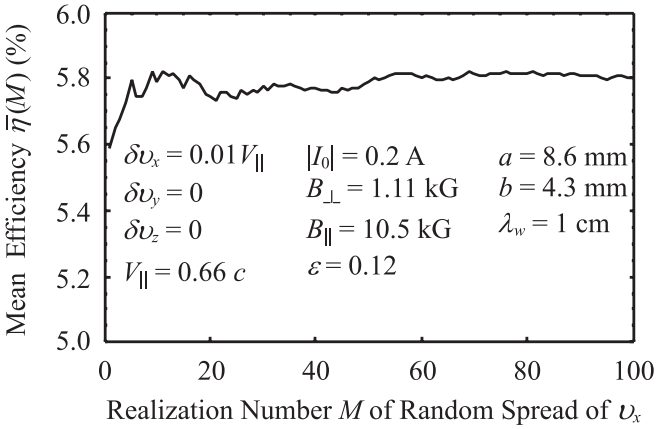

FIG. 14. The saturation efficiency averaged over realizations of random v_x versus the realization number M.

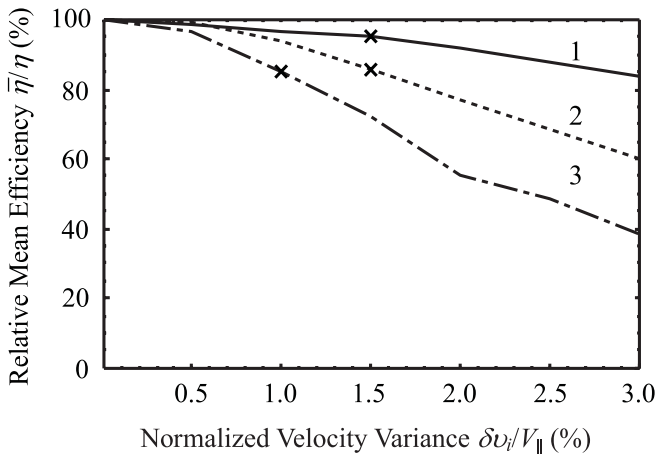

FIG. 15. The mean saturation efficiency versus the normalized velocity variance. Curve 1 corresponds to the case when the only v_x spread is taken into account while $\delta v_y = \delta v_z = 0$, curve 2 corresponds to the case when the only v_y spread is taken into account while $\delta v_x = \delta v_z = 0$, and curve 3 corresponds to the case when the only v_z spread is taken into account while $\delta v_x = \delta v_y = 0$.

This, in our view, nontrivial observation greatly simplifies calculations of mean efficiency. Then, for example, using Fig. 15, if $\delta v_x = \delta v_y = 0.015 V_\parallel$ and $\delta v_z = 0.01 V_\parallel$ one can determine the relative mean efficiency as $\bar{\eta}(\delta v_x, \delta v_y, \delta v_z)/\eta(0,0,0) \approx 0.69$. Besides, we find that the initial spread of the z component of velocity is more critical for the saturation efficiency than those of x and y components because of predominantly axial bunching mechanism. It also follows from the results shown in Figs. 15 and 16 that the influence of initial velocity spread is weak if the normalized variance $\delta v/V_\parallel = (\delta v_x^2 + \delta v_y^2 + \delta v_z^2)^{1/2}/V_\parallel$ is much less than the (ideal) efficiency $\eta(0,0,0)$. Figure 16 illustrates that the (near) magnetoresonant regime of operation of a hybrid planar FEM is preferable to any other operation regime even if the initial beam velocity spread is taken into account (cf. also Fig. 13).

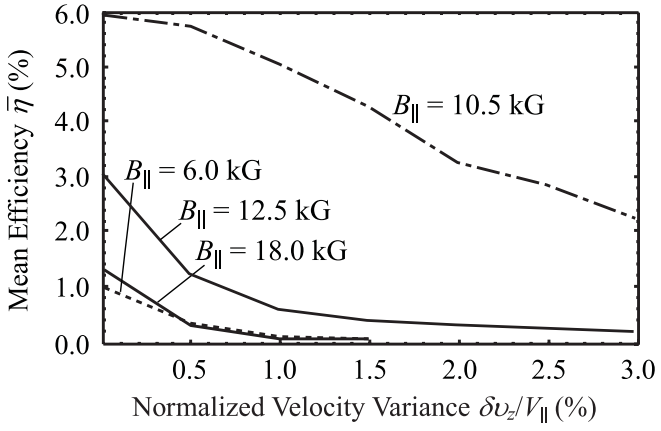

FIG. 16. The mean saturation efficiency for different $B_\parallel$ versus the normalized velocity variance.

Summing up this section, we numerically verified that neither inhomogeneity of undulator magnetic field and adiabatic entrance section nor space-charge effects and initial beam velocity spread influence critically the (near) magnetoresonant regime of operation of a hybrid planar FEM proposed in Sec. III.

VI. CONCLUSIONS

We applied Kisunko-Vainshtein's equations of excitation for regular waveguides to the development of a self-consistent analytical linear theory of a hybrid planar FEM amplifier, which is valid not only far away but also around the magnetoresonant value of the guide magnetic field ($\Omega_\parallel \approx \Omega_0$). Nonlinear numerical simulations were undertaken to clarify the validity of the linear approximation. Although, as mentioned at the beginning of this article, a number of approaches to the linear theory of a hybrid FEM have been already formulated, a new one presented here allowed us to both provide a consistent and unified analytical description of electron dynamics for all values of the guide magnetic field and, more importantly, to find an efficient characterization of the dynamical chaos present in the system. It is also worth mentioning that the zones of suppressed beam transport found in [12] are in good correspondence with our (semi)analytical calculations for the zones of dynamical chaos (cf. Fig. 1 in [12] and Figs. 2 and 5 of this article). This is achieved because the method of Lindshtedt employed by us to obtain test individual electron trajectories in the magnetostatic field of a hybrid planar FEM is capable of high precision in analytical calculations. It should be also mentioned that this method is sufficiently general to be applicable to describe the motion of charged particles in spatially inhomogeneous static magnetic fields like, for example, that in [12,29].

The origin of dynamical chaos is connected to the possibility of the onset of a stochastic layer around the separatrix in the system phase space [under the condition $\omega_\perp/\omega_0 = [(1 + V_x^2/V_\parallel^2)^{1/2} + V_x/V_\parallel]/2$ motion of an electron in the undulator magnetic field takes place along the separatrix] caused by the presence of the guide magnetic field, which plays the role of a nontrivial perturbation capable of destruction of this separatrix. The magnitude and sign of the x component of the initial velocity of electrons influence the position of the separatrix in the phase space and allows one to adjust the location of zones of regular and chaotic dynamics when the guide magnetic field is present. An approximate condition that determines the onset of chaos is given analytically and found to be in good quantitative agreement with numerical simulations. The chaotic behavior occurs whenever the absolute value of the difference between the normal undulator, Ω_0, and normal cyclotron, $\Omega_\parallel$, frequencies becomes less than the coupling, $\omega_\perp$, induced by the undulator magnetic field.

From linearized in the microwave field equations of motion and excitation a dispersion equation is derived for the undulator synchronism. We showed analytically that around the magnetoresonance on the undulator synchronism the gain is nearly completely independent of the amplitude of the undulator magnetic field. This circumstance is known in the literature but only as a result of numerical simulations (cf. Fig. 2 in [47]). The physical origin of this effect lies in the fact that the gain is a function of amplitude of transversal oscillations of electrons in the magnetostatic field of a hybrid planar FEM. Around the magnetoresonant value of the guide magnetic field this amplitude, according to the chaotization criterium (8), turns out to be bounded and is independent of the amplitude of the undulator magnetic field. The obtained analytical expression for the gain provides values in good agreement with results of nonlinear numerical simulations even when a more realistic assumption on the inhomogeneity of undulator magnetic field and adiabatic entrance of electron beam to the interaction region is taken into account. The interaction between transversal degrees of freedom of electrons and microwave field in the (near) magnetoresonant regime turns out to be maximal out of all other possible operation parameters of a hybrid planar FEM (experimentally for a hybrid planar FEM oscillator such an operational regime was established, for example, in [13]). The major result here is that one needs not only to have a small value of ε in order to maintain the relation $\bar{v}_{\parallel} \gg \bar{v}_{\perp}$ ($\bar{v}_{\perp}$ is the mean transversal velocity) but also to hold the ratio $\varepsilon/|\kappa - \sigma| \equiv \omega_{\perp}/|\Omega_0 - \Omega_{\parallel}|$ as close to the unity as possible thus providing for the maximal gain and efficiency.

Numerical calculations were accomplished to study space-charge effects and the influence of initial beam velocity spread on microwave amplification of a hybrid planar FEM. It is found that the rotational part of the nonradiated (space-charge) field suppresses the defocusing caused by its potential part and for the guide magnetic field values slightly above the upper edge of the chaotic dynamics zone the influence of the space-charge field on microwave amplification is much less than for its values far away from the magnetoresonance. The influence of the initial beam velocity spread is weak if the normalized variance of velocity is much less than the ideal efficiency (i.e. the efficiency calculated neglecting the initial beam velocity spread) and the (near) magnetoresonant regime of operation of a hybrid planar FEM is preferable to any other operation regime even if the initial beam velocity spread is taken into account (see Fig. 16).

Summarizing, our numerical simulations confirm that the presence of an adiabatic entrance section and initial beam velocity spread or space-charge effects does not alter the analytical conclusions on the advantage of the (near) magnetoresonant regime of operation of a hybrid planar FEM.

ACKNOWLEDGMENTS

We acknowledge fruitful conversations and discussions with K. Yu. Bliokh, V. L. Bratman, N. S. Ginzburg, N. Yu. Peskov, O. V. Usatenko, and V. V. Yanovsky. We are also grateful to anonymous referees, whose considered criticism allowed us to improve the exposition substantially.

[1] P. Sprangle and V. L. Granatstein, Phys. Rev. A **17**, 1792 (1978).
[2] R. K. Parker, R. H. Jackson, S. H. Gold, H. P. Freund, V. L. Granatstein, P. C. Efthimion, M. Herndon, and A. K. Kinkead, Phys. Rev. Lett. **48**, 238 (1982).
[3] J. Andruszkow *et al.*, Phys. Rev. Lett. **85**, 3825 (2000).
[4] M. A. Agafonov, A. V. Arzhannikov, N. S. Ginzburg, V. G. Ivannenko, P. V. Kalinin, S. A. Kuznetsov, N. Y. Peskov, and S. L. Sinitsky, IEEE Trans. Plasma Sci. **26**, 531 (1998).
[5] W. H. Louisell, J. F. Lam, D. A. Copeland, and W. B. Colson, Phys. Rev. A **19**, 288 (1979).
[6] H. P. Freund, P. Sprangle, D. Dillenburg, E. H. da Jornada, B. Liberman, and R. S. Schneider, Phys. Rev. A **24**, 1965 (1981).
[7] S. S. Kokhmanskii and V. V. Kulish, Acta Phys. Pol. A **66**, 713 (1984).
[8] J. Masud, T. C. Marshall, S. P. Schlesinger, and F. G. Yee, Phys. Rev. Lett. **56**, 1567 (1986).
[9] N. S. Ginzburg and Y. V. Novozhilova, Sov. Phys. Tech. Phys. **31**, 1017 (1986).
[10] M. E. Conde and G. Bekefi, Phys. Rev. Lett. **67**, 3082 (1991).
[11] Y. B. Viktorov, A. B. Draganov, A. K. Kaminsky, N. Y. Kotsarenko, S. B. Rubin, V. P. Sarantsev, A. P. Sergeev, and A. A. Silivra, Zh. Tekh. Fiz. **61**, 133 (1991).
[12] K. Sakamoto, T. Kobayashi, Y. Kishimoto, S. Kawasaki, S. Musyoki, A. Watanabe, M. Takahashi, H. Ishizuka, and M. Shiho, Phys. Rev. Lett. **70**, 441 (1993).
[13] V. L. Bratman, G. G. Denisov, N. S. Ginzburg, B. D. Kol'chugin, N. Y. Peskov, S. V. Samsonov, and A. B. Volkov, IEEE Trans. Plasma Sci. **24**, 744 (1996).
[14] C. Chen and R. C. Davidson, Phys. Rev. A **42**, 5041 (1990).
[15] C. Chen and R. C. Davidson, Phys. Rev. A **43**, 5541 (1991).
[16] L. Michel, A. Bourdier, and J. M. Buzzi, Nucl. Instrum. Methods Phys. Res., Sect. A **304**, 465 (1991).
[17] L. Michel-Lours, A. Bourdier, and J. M. Buzzi, Phys. Fluids B **5**, 965 (1993).
[18] H. P. Freund and T. M. Antonsen, *Principles of Free-Electron Lasers* (Chapman & Hall, New York, 1995).
[19] B. P. Yefimov, K. V. Ilyenko, T. Y. Yatsenko, and V. A. Goryashko, Telecommun. Radio Eng. **61**, 243 (2004).
[20] A. A. Kuraev, N. A. Kuraev, and A. K. Sinitsyn, Radiotekh. Elektron. **36**, 2179 (1991).
[21] Y. Pinhasi and A. Gover, Phys. Rev. E **51**, 2472 (1995).
[22] J. Larsson, Am. J. Phys. **75**, 230 (2007).
[23] N. M. Sovetov, *Analysis and Desing of Travel Wave Tube and Its Hybrids By Phase-Plane Method* (Saratov

University Press, Saratov, USSR, 1974), in Russian.
[24] G. V. Kisunko, *Electrodynamics of Hollow Structures* (RedBanner Military Academy of Communications, Leningrad, USSR, 1949), in Russian.
[25] L. A. Vainshtein and V. A. Solntsev, *Lectures on High-Frequency Electronics* (Soviet Radio, Moscow, USSR, 1973), in Russian.
[26] A. V. Gaponov, Izv. Vyssh. Uchebn. Zaved., Radiofiz. **4**, 547 (1961).
[27] A. A. Kuraev, *Ultrahighfrequency Devices with Periodic Electron Flows* (Science and Engineering, Minsk, USSR, 1971), in Russian.
[28] H. P. Freund, H. Bluem, and C. L. Chang, Phys. Rev. A **36**, 2182 (1987).
[29] S. Cheng, W. W. Destler, V. L. Granatstein, T. M. Antonsen, B. Levush, J. Rodgers, and Z. X. Zhang, IEEE Trans. Plasma Sci. **24**, 750 (1996).
[30] L. Friedland and J. L. Hirshfield, Phys. Rev. Lett. **44**, 1456 (1980).
[31] W. B. Colson, IEEE J. Quantum Electron. **17**, 1417 (1981).
[32] V. I. Arnold, *Mathematical Aspects of Classical and Celestial Mechanics* (Springer-Verlag, Berlin, Germany, 1993).
[33] V. V. Kozlov, *General Theory of Vortices* (Regular and Chaotic Dynamics, Izhevsk, Russia, 1998), in Russian.
[34] A. Lindshtedt, Memoirs l'Acad. Sci. St.-Peterbourg. **31**, 1 (1883).
[35] A. Blaquiere, *Nonlinear System Analysis* (Academic Press, New York, 1966).
[36] M. I. Rabinovich and D. I. Trubetskov, *Oscillations and Waves in Linear and Nonlinear Systems* (Kluwer Academic, Dordrecht, Germany, 1989).
[37] R. Z. Sagdeev, D. A. Usikov, and G. M. Zaslavsky, *Nonlinear Physics : From The Pendulum to Turbulence and Chaos* (Harwood Academic, New York, 1988).
[38] A. Grossman, T. C. Marshall, and S. P. Schlesinger, Phys. Fluids **26**, 337 (1983).
[39] B. V. Chirikov, Phys. Rep. **52**, 263 (1979).
[40] V. V. Kozlov, Russ. Math. Surv. **38**, 1 (1983).
[41] V. A. Goryashko, K. V. Ilyenko, and A. N. Opanasenko, Radiofiz. Elektronika **11**, 440 (2006).
[42] V. L. Bratman, N. S. Ginzburg, and M. I. Petelin, JETP Lett. **28**, 190 (1978).
[43] H. Haken, *Advanced Synergetics* (Springer-Verlag, Berlin, Germany, 1983).
[44] V. Goryashko, K. Ilyenko, and A. Opanasenko, Proceedings of the Eighth IEEE International Vacuum Electronics Conference, Kitakyushu, Japan, 2007, p. 291.
[45] A. K. Ganguly and H. P. Freund, Phys. Rev. A **32**, 2275 (1985).
[46] H. P. Freund and A. K. Ganguly, Phys. Rev. A **33**, 1060 (1986).
[47] N. S. Ginzburg, R. M. Rozental, N. Y. Peskov, A. V. Arzhannikov, and S. L. Sinitskii, Phys. Tech. J. **46**, 1545 (2001).